PCCP

ROYAL SOCIETY OF CHEMISTRY

PAPER

View Article Online
View Journal | View Issue

Check for updates

Cite this: *Phys. Chem. Chem. Phys.*, 2024, **26**, 25678

Rotational conformers and nuclear spin isomers of carbonyl diisothiocyanate†

Eva Gougoula, *[a] Jonathan Pfeiffer,[b] Melanie Schnell *[ac] and Frank Tambornino *[b]

Received 30th May 2024,
Accepted 16th September 2024

DOI: 10.1039/d4cp02226b

rsc.li/pccp

Published on 18 September 2024. Downloaded on 04.02.2026 19:17:07.

Nuclear spin isomers of molecules play a pivotal role in our understanding of quantum mechanics and can have significant implications for various fields. In this work, we report the isolation and characterization of stable nuclear spin isomers as well as conformational isomers of a reactive compound, namely carbonyl diisothiocyanate. It can exist as three rotational conformers, two of which, the *syn–syn* and *syn–anti*, were observed in a pulsed supersonic jet by chirped pulse Fourier transform microwave spectroscopy in the 2–12 GHz frequency region. The rotational spectra of two distinct nuclear spin isomers of *syn–syn*-carbonyl diisothiocyanate, *ortho* and *para*, were recorded and analyzed. Experimental molecular rotational parameters for the identified rotational and nuclear spin isomers were determined, including rotational constants, centrifugal distortion constants, and nuclear quadrupole coupling constants. The two nuclear spin isomers are distinguished by unique hyperfine splitting signatures in their rotational spectra as an outcome of their different nuclear spin states. The relative abundances of the two observed conformers in the gas phase were estimated from the intensity of their rotational transitions. Following detection of singly substituted rare isotopologues of the *syn–syn* conformer, a partial substitution (r_s) structure was determined.

Introduction

Molecules with equivalent nuclei with non-zero spin can exist as nuclear spin isomers which are characterized by different sets of rotational quantum numbers that they are allowed to populate.[1] Nuclear spin isomers have a pivotal role in the manifestation of quantum mechanics and our understanding of fundamental science as well as across various disciplines. To name a few, the unique properties of nuclear spin isomers may find potential applications in quantum computing,[2,3] medical imaging,[4,5] and astrophysics where the measured ratios between different nuclear spin isomers can provide an insight into astrophysical processes and stellar environments.[6–8] The first observation of nuclear spin isomers was reported in 1929[9] with the separation and interconversion of *ortho*- and *para*-H_2, where the orientation of the spin of each hydrogen can be parallel or anti-parallel, respectively. Separation and conversion of nuclear spin isomers was later observed for a number of other molecules, *e.g.* water,[10,11] methanol,[12] ethylene,[13–15] and fluoromethane,[16,17] to name a few. However, in the gas phase, the interconversion between isomers is generally considered improbable, and thus spectroscopic studies in the gas phase can be an ideal way to study isolated nuclear spin isomers.

Advances in modern synthetic chemistry play a key role in engineering molecules with unique symmetry properties that can serve as prototypes to study the properties of isolated nuclear spin isomers. Carbonyl diisothiocyanate (CDIT, C═O(NCS)$_2$), a reactive compound that consists of a carbonyl (C═O) and two isothiocyanate groups (–N═C═S), was first reported in 1902,[18] and reliable synthetic routes to its formation were established in 1981[19,20] and reinvestigated in 2021.[21] In principle, the compound can exist as three different rotational conformers (Fig. 1), *syn–syn*, *syn–anti*, and *anti–anti* (with respect to the carbonyl bond relative to the heterocumulene). Additionally, it consists exclusively of non-hydrogen atoms, all of which have a nuclear spin (I) of 0 or 1, and thus are bosons. In the *syn–syn* and *anti–anti* forms, due to the overall symmetry of the molecules, the atoms of the –NCS groups are equivalent upon exchange and Bose–Einstein statistics are expected to influence their rotational spectra.

Information on the structure and relative conformational abundances of carbonyl diisocyanate (C═O(NCO)$_2$)[22,23] and carbonyl diazide (C═O(N$_3$)$_2$)[24] is available through gas-phase electron diffraction (GED) and infrared (IR) spectroscopy.

[a] *Deutsches-Elektronen Synchrotron DESY, Notkestr. 85, 22607 Hamburg, Germany. E-mail: eva.gougoula@desy.de, melanie.schnell@desy.de*
[b] *Fachbereich Chemie, Philipps-Universität Marburg, Hans-Meerwein-Straße 4, 35043 Marburg, Germany. E-mail: tamborni@chemie.uni-marburg.de*
[c] *Institut für Physikalische Chemie, Christian-Albrechts-Universität zu Kiel, 24118 Kiel, Germany*

† Electronic supplementary information (ESI) available. See DOI: https://doi.org/10.1039/d4cp02226b

This journal is © the Owner Societies 2024

Published on 18 September 2024. Downloaded on 04.02.2026 19:17:07.

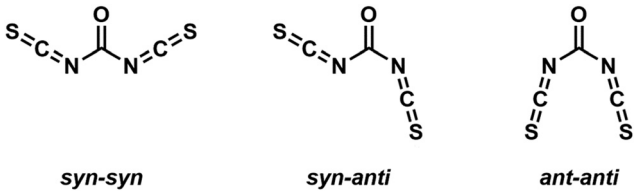

Fig. 1 Possible conformers of carbonyl dipseudohalides (*syn–syn*, *syn–anti*, and *anti–anti*) illustrated by the example of carbonyl diisothiocyanate. *syn*: carbonyl group and isothiocyanate group on the same side, *anti*: carbonyl group and isothiocyanate group on different sides.

The two are closely related to CDIT, both in terms of the available conformations they can adopt, but also by possessing isoelectronic functional groups attached to the carbonyl, and displaying high reactivity. Both the *syn–syn* and *syn–anti* forms have been characterized for C═O(NCO)$_2$ and C═O(N$_3$)$_2$, with the *syn–syn* form being the dominant species in both cases, an observation that is also supported by quantum chemical calculations. Condensed phase studies on CDIT with X-ray diffraction (XRD) only identified the *syn–syn* conformer in the crystal, which is also the most stable form. An important step towards characterizing and rationalizing the properties of CDIT is to obtain spectroscopic insight into the *syn–anti* conformation, as well as to experimentally determine its conformational preferences.

In this work, we report the rotational spectrum of CDIT in the gas phase using chirped pulse Fourier transform microwave (CP-FTMW) spectroscopy. The *syn–syn* and *syn–anti* conformations are detected, providing access to the molecular properties of the elusive conformer. Their relative abundances fall within the broader expectations based on similar systems and on their computed energies. Interesting effects are observed in the spectrum of the *syn–syn* conformer consistent with the presence of two distinct nuclear spin isomers that follow nuclear spin statistics for bosons. The structure of *syn–syn*-CDIT was partially determined through isotopic substitution of the atoms in the –NCS groups.

Results and discussion

The three possible conformers of CDIT (Fig. 1), *syn–syn*, *syn–anti*, and *anti–anti*, arise through rotation of the isothiocyanate groups –N═C═S around the C2–N6 or C2–N3 bonds (see Fig. 1 for atom labeling), respectively. The calculated molecular parameters of the conformers of CDIT (Table 1) show that the *syn–syn* and *syn–anti* conformers are near-prolate asymmetric tops. The potential energy surface connecting the three possible conformers is calculated at the PBEh-3c level of theory. The two conformers are separated by a high energy barrier ($\sim$16 kJ mol^{-1}), with *syn–anti*-CDIT lying approximately 4.5 kJ mol^{-1} higher than *syn–syn*-CDIT, the global minimum. *Anti–anti*-CDIT is a near-oblate asymmetric top, and it is calculated to be approximately 9.5 kJ mol^{-1} higher in energy than *syn–syn*-CDIT. All three conformers have a sizeable electric dipole moment component along the *b*-axis of inertia. In *syn–syn*- and *anti–anti*-CDIT, due to symmetry, the C_2 axis is aligned with the *b*-axis of inertia and the C═O bond, which results in three equivalent pairs of atoms between the two isothiocyanate –N═C═S groups (Fig. 2).

Table 1 Calculated rotational parameters, including nuclear quadrupole coupling constants of the two ^{14}N nuclei and relative energies of the three possible conformers of CDIT obtained at the B3LYP-D3(BJ)/aug-cc-pVTZ level

	syn–syn	*syn–anti*	*anti–anti*
A_e (MHz)	10 335.6	2901.6	1425.6
B_e (MHz)	443.7	612.0	1165.6
C_e (MHz)	425.4	505.4	641.3
$\chi_{aa}(N_3)$ (MHz)	1.763	1.618	1.861
$\chi_{bb}(N_3)-\chi_{cc}(N_3)$ (MHz)	0.936	–1.030	0.823
$\chi_{aa}(N_6)$ (MHz)	1.763	0.245	1.861
$\chi_{bb}(N_6)-\chi_{cc}(N_6)$ (MHz)	0.936	0.742	0.823
$\lvert\mu_a\rvert$, $\lvert\mu_b\rvert$, $\lvert\mu_c\rvert$ (D)	0, 1.2, 0	0.4, 2.2, 0	0, 2.6, 0
κ^a	–0.99	–0.91	0.34
$\Delta E_{rel}{}^b$ (cm^{-1}, kJ mol^{-1})	0	377.4, 4.5	791.9, 9.5
$\Delta E_{barrier}{}^c$ (cm^{-1}, kJ mol^{-1})	1305, 16	1190, 14	

^{a} Ray's asymmetry parameter $\kappa = \frac{2B-A-C}{A-C}$. ^{b} Relative energies calculated with respect to *syn–syn*-CDIT at the B3LYP-D3(BJ)/aug-cc-pVTZ level. ^{c} Energy barriers between *syn–syn*-CDIT and *syn–anti*-CDIT, and *syn–anti*-CDIT and *anti–anti*-CDIT obtained at the PBEh-3c level and reported with respect to the energetically lower of the two minima it separates, and shown with respect to the relative energies of the conformers at the same level of theory.

Spectrum of *syn–syn*-CDIT

The jet-cooled rotational spectrum of CDIT was collected over the 2–12 GHz frequency range, in segments of 2–8 and 8–12 GHz. Upon initial inspection of the 8–12 GHz region, the most intense feature is a pattern consistent with a b-type, *Q*-branch transition. The lines exhibit hyperfine splitting as expected for a molecule with one or two N nuclei with nuclear spin I = 1. Watson's *S*-reduction,[25] as implemented in Western's PGOPHER,[26] was used to perform the initial assignment of the spectrum, without consideration of the hyperfine splitting. The $1_{1,0} \leftarrow 1_{0,1}$ transition was identified at approximately 10 615 MHz which gave an excellent initial value of the A_0 rotational constant. A preliminary fit including b-type, *Q*-, *P*-, and *R*-branch transitions was performed and yielded the initial set of the A_0, B_0, and C_0 rotational constants which were assigned to *syn–syn*-CDIT, based on agreement (see Table S1, ESI†) between the calculated and experimentally determined rotational constants.

Upon inclusion of the nuclear quadrupole coupling terms $\chi_{aa}(^{14}N)$ and $\chi_{bb}(^{14}N)-\chi_{cc}(^{14}N)$ in the fit, the experimental hyperfine splitting appears to vary. For some transitions, it appears to be consistent with one N nucleus (I = 1), while for others with two N (I_1 = 1 and I_2 = 1) nuclei. In order to rationalize which types of transitions appear to have splitting equivalent to one or two quadrupolar nuclei, two separate fits, Fit 1 and Fit 2, grouping the different types of transitions were performed with PGOPHER,[26] and the experimentally determined spectroscopic parameters are summarized in Table S2 (ESI†). The types of transitions, *Q*-, *P*-, and *R*-branch, with odd or even $K''_{sum} = K''_a + K''_c$, that were included in each fit are indicated in the last rows of Table S2 (ESI†). The hyperfine

Published on 18 September 2024. Downloaded on 04.02.2026 19:17:07.

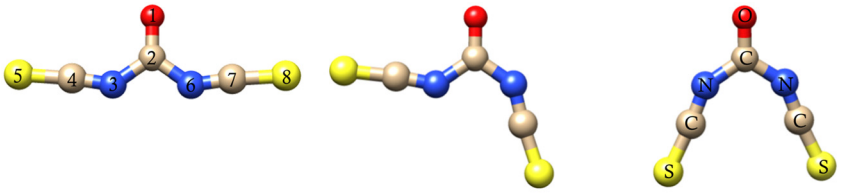

syn-syn-CDIT | *syn-anti*-CDIT | *anti-anti*-CDIT

0 (cm^{-1}, kJ mol^{-1}) | 377.4, 4.5 | 791.9, 9.5

Fig. 2 Optimized (r_e) geometries and relative energies of the three possible conformers of CDIT calculated at the B3LYP-D3(BJ)/aug-cc-pVTZ level.

splitting of some representative rotational transitions is showcased in the expanded part of Fig. 3. The two fits yield similar rotational constants which are within the standard deviation of each other, thus excluding the possibility that the variation in the hyperfine splitting is associated with a large amplitude motion within the molecule. This is further supported by the value of D_{JK}, which is in the range of just a couple of kHz. Regarding the nuclear quadrupole coupling constants of the two fits, these are of similar magnitude, however, their signs are reversed as an outcome of only considering one coupling nucleus in Fit 1. These observations suggest that there are two nuclear spin isomers of *syn–syn*-CDIT, *ortho* and *para*, associated with nuclear spin states of I = 0, 2 and I = 1, respectively, and nuclear spin statistics dictate the allowed and forbidden transitions. For the *ortho* isomer, energy levels with even values of K''_{sum} have a non-zero statistical weight, and those with odd values a zero statistical weight, while for the *para* isomer the opposite is observed. A more detailed explanation on the spin states and the assignment of transitions to the *ortho* and *para* isomers will follow in the coming paragraphs.

Following the work of Grubbs *et al.*,[27] it is possible to perform a global fit that includes transitions of both *ortho*- and *para*-(*syn–syn*-CDIT) using Pickett's SPFIT/SPCAT.[28] Watson's *S*-reduced Hamiltonian[25] as implemented in SPFIT was used in the form:

$$\hat{H}_{TOT} = \hat{H}_{ROT} + \hat{H}_{CD} + \hat{H}_{Q}(N) + \hat{H}_{SS}(N)$$

where $\hat{H}_{ROT}$, $\hat{H}_{CD}$, $\hat{H}_{Q}$, and $\hat{H}_{SS}$ are the rotational, centrifugal distortion, nuclear quadrupole coupling, and nuclear spin–nuclear spin coupling terms, respectively. The high degree of similarity between the rotational and centrifugal distortion constants of the two nuclear spin isomers (see Table S2, ESI†) allows for simultaneous fitting of the $\hat{H}_{ROT}$ and $\hat{H}_{CD}$ terms to both isomers, yielding average values for these constants. The $\hat{H}_{Q}$ term was fitted according to the coupling scheme $I_{N_3} + I_{N_6} = I_{tot}$ and $J + I_{tot} = F$, which implies coupling between two equivalent quadrupolar nuclei. The results of this fit are summarized in Table 2 and are consistent with those of Table S2 (ESI†). The nuclear spin–nuclear spin coupling term is inseparable from the nuclear quadrupole coupling term, and therefore determination of $\hat{H}_{Q}$ is a linear combination of the

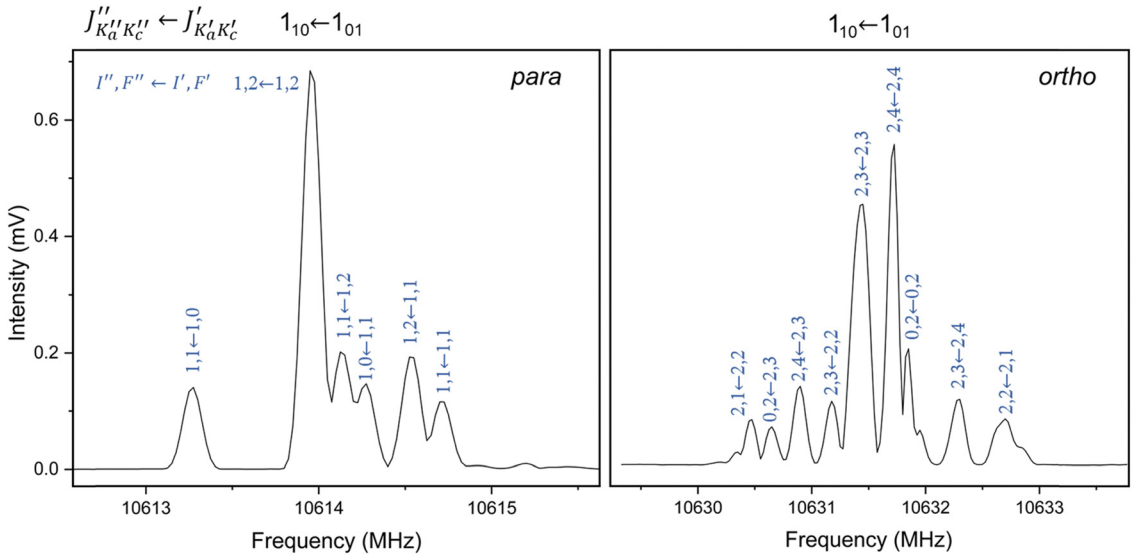

Fig. 3 Representative rotational transitions $J''_{K''_a K''_c} \leftarrow J'_{K'_a K'_c}$ of *ortho*- and *para*-(*syn–syn*-CDIT) carrying hyperfine splitting due to ^{14}N nuclei. The splitting in the spectrum of the *para* isomer is consistent with one ^{14}N nucleus, while that for the *ortho* isomer is analogous to two ^{14}N nuclei. Some I″, F″ ← I′, F′ hyperfine transitions are annotated, respectively.

 This journal is © the Owner Societies 2024

Published on 18 September 2024. Downloaded on 04.02.2026 19:17:07.

Table 2 Final fits of the rotational spectra of *syn–syn* and *syn–anti*-CDIT performed with SPFIT/SPCAT using Watson's *S*-reduction

	syn–syn-CDIT $I_{N_3} + I_{N_6} = I_{tot}$	*syn–anti*-CDIT
A_0[a] (MHz)	11 046.3581(24)[b]	2938.6797(15)
B_0 (MHz)	449.80178(41)	626.51962(71)
C_0 (MHz)	432.27083(56)	516.14194(50)
D_J[c] (kHz)	—	0.2008(52)
D_{JK} (kHz)	1.281(38)	−3.099(39)
D_K (kHz)	—	−20.74(16)
d_1 (kHz)	—	−0.0779(19)
$\chi_{aa}(N_3)$[d] (MHz)	1.9269(56)	1.745(11)
$\chi_{bb}(N_3)-\chi_{cc}(N_3)$ (MHz)	−0.742(10)	−0.634(14)
$\chi_{aa}(N_6)$ (MHz)	1.9269(56)	0
$\chi_{bb}(N_6)-\chi_{cc}(N_6)$ (MHz)	−0.742(10)	0.881(17)
$\lvert\mu_a\rvert, \lvert\mu_b\rvert, \lvert\mu_c\rvert$[e] (D)	0, 1.2, 0	0.4, 2.2, 0
a-/b-/c-Type[f]	N/Y/N	N/Y/N
κ[g]	−0.99	−0.91
N[h]	177	161
σ_{RMS}[i] (kHz)	13.2	16.3

[a] A_0, B_0, C_0: experimentally determined rotational constants simultaneously determined for the *ortho* and *para* nuclear spin isomers of the *syn–syn*-CDIT conformer, and for the *syn–anti*-CDIT conformer. [b] Numbers in parentheses are one standard deviation in units of the last significant figures. [c] D_J, D_{JK}, D_K, d_1: quartic centrifugal distortion constants simultaneously determined for the *ortho* and *para* nuclear spin isomers of the *syn–syn*-CDIT conformer, and for the *syn–anti*-CDIT conformer, respectively. [d] χ_{aa} and $\chi_{bb}-\chi_{cc}$: nuclear quadrupole coupling constants. [e] Magnitude of the calculated dipole moment components. [f] a-/b-/c-Type transitions. Y and N correspond to "yes" and "no", respectively, indicating whether the type of transition is detected. [g] Ray's asymmetry parameter $\kappa = \frac{2B-A-C}{A-C}$. [h] Number of assigned rotational transitions, including hyperfine transitions. [i] Root mean square deviation of the fit.

two.[29] As mentioned, there are two nuclear spin wavefunctions that describe the *ortho* isomer, however, the lines that belong to the $I = 0$ state exhibit significant overlap and blending with the $I = 2$ lines. In the current fit, only a handful of well-resolved and well-isolated lines of the $I = 0$ state were identified. The detailed operator codes that were used for this fit and a complete line list are given in the ESI.†

The assignment of transitions to the *ortho* and *para* nuclear spin isomers of *syn–syn*-CDIT was based on arguments around nuclear spin statistics, appropriate for the exchange of multiple pairs of bosons. The C_{2v} symmetry of this conformer implies that rotation about the *b*-axis, which coincides with the C_2 axis, interchanges equivalent bosons. It holds that the total wavefunction:

$$\psi_{tot} = \psi_{elec} \times \psi_{vib} \times \psi_{rot} \times \psi_{ns} \quad (1)$$

where ψ_{elec}, ψ_{vib}, ψ_{rot}, and ψ_{ns} are the electronic, vibrational, rotational, and nuclear spin wavefunctions, respectively, is symmetric and of positive parity. Thus, upon C_2 rotation, *i.e.*, exchange of identical bosons, we have:

$$\psi(2, 1) = +\psi(1, 2) \quad (2)$$

Considering that our experiment probes the vibronic ground state, the electronic and vibrational wavefunctions for *syn–syn*-CDIT both have a positive parity. Therefore, the total parity of ψ_{tot} is determined by the product of $\psi_{rot} \times \psi_{ns}$ such that:

$$\psi_{tot} = \begin{cases} \psi_{rot}^{(+)} \times \psi_{ns}^{(+)} \\ \text{or} \\ \psi_{rot}^{(-)} \times \psi_{ns}^{(-)} \end{cases} \quad (3)$$

where the symbols in parentheses indicate the parity. Upon a C_2 rotation about the symmetry axis, the rotational wavefunction is multiplied by $(-1)^{K''_{sum}}$. The parity of ψ_{rot} depends on the sum of $K''_a + K''_c = K''_{sum}$, specific to each $J'' \leftarrow J'$ rotational transition, such that:

$$\psi_{rot} = \begin{cases} \psi_{rot}^{(+)} \sim (-1)^{2n} \\ \text{or} \\ \psi_{rot}^{(-)} \sim (-1)^{(2n+1)} \end{cases} \quad (4)$$

For even $K''_{sum}(2n)$ the parity of ψ_{rot} is positive and for odd $K''_{sum}(2n+1)$ the parity of ψ_{rot} is negative. From eqn (3) and (4) it follows that ψ_{ns} must be of positive parity (*ortho*-isomers) for even K''_{sum} and of negative parity (*para*-isomers) for odd K''_{sum}. The ratio between symmetric and antisymmetric nuclear spin wavefunctions is given by:

$$\frac{N_+}{N_-} = \frac{(I+1)(2I+1)}{I(2I+1)} = \frac{I+1}{I} \quad (5)$$

There are two symmetric and one antisymmetric spin wavefunctions, corresponding to two *ortho*-isomers (I_{tot} = 0, 2), associated with even K''_{sum}, and one *para*-isomer (I_{tot} = 1), associated with odd K''_{sum}.

Sufficient signal to noise ratio for several rotational transitions of the parent *syn–syn*-CDIT allowed for detection of the singly substituted ^{34}S, ^{13}C, and ^{15}N isotopologues in their natural isotopic abundances, 4.4%, 1.1%, and 0.4%, respectively. Detection of these isotopologues further confirms the assignment of the fitted rotational constants to *syn–syn*-CDIT. The C_2 axis of symmetry renders the atoms of the two isothiocyanate groups equivalent to each other which results in doubling of the signal intensity of the respective singly substituted isotopologue. It should be noted that it is possible to perform a global fit for each rare isotopologue, including all the available transitions. Single isotopic substitution reduces the C_{2v} symmetry to C_s, meaning that the N, C, and S atoms are no longer equivalent. This holds as further evidence that the observed spectral behavior of the parent *syn–syn*-CDIT isotopologue is an outcome of the presence of two distinct nuclear spin isomers.

The fitted spectroscopic parameters of the singly substituted ^{34}S, ^{13}C, and ^{15}N isotopologues of *syn–syn*-CDIT are collected in Table 3. To generate these parameters, a pseudo-C_{2v}‡ geometry is assumed. Attempts to treat the symmetry as C_s with non-

‡ Single isotopic substitution reduces the symmetry of *syn–syn*-CDIT from C_{2v} to C_s, making the atoms in the –N═C═S groups non-equivalent. Pseudo-C_{2v} refers to the treatment of the C_s as C_{2v} for the sake of obtaining a fit that can converge with reasonable values of nuclear quadrupole coupling constants.

Published on 18 September 2024. Downloaded on 04.02.2026 19:17:07.

Table 3 Experimentally determined spectroscopic parameters of the singly substituted ^{34}S, ^{13}C, and ^{15}N isotopologues of *syn–syn*-CDIT in their natural isotopic abundances

	^{34}S	^{13}C	^{15}N
A_0 (MHz)	11 042.9488(27)[a]	11 029.0588(35)	11 002.9140(90)
B_0 (MHz)	438.30798(69)	447.6461(18)	449.3334(98)
C_0 (MHz)	421.6377(14)	430.2687(18)	431.7588(90)
D_{JK} (kHz)	1.86(24)	[1.86]	[1.86]
χ_{aa}(N)[b] (MHz)	1.9870(80)	1.962(13)	[1.9870]
χ_{bb}(N)–χ_{cc}(N) (MHz)	−0.751(12)	−0.692(18)	[−0.751]
N[c]	138	66	6
σ_{RMS}[d] (kHz)	14.4	14.9	10.8

[a] Numbers in parentheses are one standard deviation in units of the last significant figures. [b] Two equivalent nitrogen atoms assumed in the fits of the ^{34}S and ^{13}C isotopologues. Only one quadrupolar nucleus is considered for the ^{15}N isotopologue. [c] Number of rotational transitions included in the fit. [d] Root mean square deviation of the fit.

equivalent N atoms prevents the fit from converging and generates unrealistically large nuclear quadrupole coupling constants in the fits for the ^{34}S and ^{13}C isotopologues. The high intensity of the spectrum of the ^{34}S isotopologue allowed for the assignment of 138 transitions, and for the determination of the quartic centrifugal distortion constant D_{JK} and nuclear quadrupole coupling constants $\chi_{aa}(^{14}\mathrm{N})$ and $\chi_{bb}(^{14}\mathrm{N})$–$\chi_{cc}(^{14}\mathrm{N})$. Unlike for the parent *syn–syn*-CDIT isotopologue, the coupling scheme $J + I_{N_3} = F_1$ and $I_{N_6} + F_1 = F$ was used to fit the nuclear quadrupole coupling constants of the ^{34}S and ^{13}C isotopologues. The D_{JK} distortion constant in the ^{13}C isotopologue fit was kept fixed to the value that was determined for the ^{34}S isotopologue. Finally, due to the small number of available transitions of the ^{15}N isotopologue, the D_{JK} and $\chi_{aa}(^{14}\mathrm{N})$ and $\chi_{bb}(^{14}\mathrm{N})$–$\chi_{cc}(^{14}\mathrm{N})$ constants were both kept fixed to the values determined for the ^{34}S isotopologue. It should be noted that only one quadrupolar nucleus is present for the ^{15}N isotopologue due to the nuclear spin of ^{15}N (I = 0). The experimentally determined A_0, B_0, and C_0 rotational constants will be used in Section 4.5 to determine the atomic coordinates of the atoms in the isothiocyanate groups in *syn–syn*-CDIT.

Spectrum of *syn–anti*-CDIT

Following the assignment of *syn–syn*-CDIT and its singly substituted ^{34}S, ^{13}C, and ^{15}N isotopologues, a large number of lines with hyperfine splitting remained unassigned. A second pattern, with significantly lower intensity than the one identified for *syn–syn*-CDIT, consistent with *Q*-branch, b-type transitions exhibiting extensive hyperfine splitting was found. Using the calculated rotational constants for *syn–anti*-CDIT as a guide, the pattern was fitted to a set of rotational parameters and allowed for identification of more lines. The final spectroscopic parameters were generated with Pickett's SPFIT/SPCAT[28] and are summarized in Table 2. The N atoms in *syn–anti*-CDIT are not equivalent, and individual $\chi_{aa}(^{14}\mathrm{N})$ and $\chi_{bb}(^{14}\mathrm{N})$–$\chi_{cc}(^{14}\mathrm{N})$ constants can be determined. The nuclear quadrupole coupling constants were fitted according to the $J + I_{N_3} = F_1$ and $I_{N_6} + F_1 = F$ coupling scheme. A representative example of fitted transitions of *syn–anti*-CDIT showcasing the hyperfine splitting is given in Fig. 4. The lower intensity of the rotational lines of *syn–anti*-CDIT did not allow for detection of singly substituted isotopologues to determine an experimental structure. However, the agreement between experimental and calculated rotational constants, the detected b-type transitions and the significantly lower intensity of this species supports the assignment to *syn–anti*-CDIT.

Relative abundances

It is immediately apparent that *syn–syn*-CDIT is the most abundant species in this experiment. This observation is in line with previous condensed phase studies on CDIT[21] and other related compounds,[24,30–33] and further supported by DFT calculations identifying this conformer as the global minimum, followed by *syn–anti*-CDIT approximately 4.5 kJ mol^{-1} higher in energy. The relative abundances of *syn–syn* and *syn–anti*-CDIT

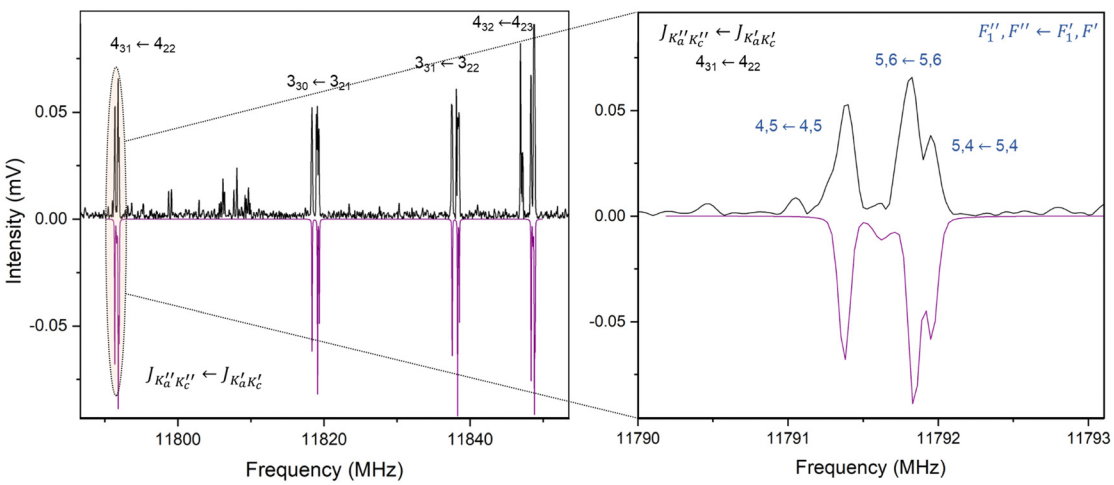

Fig. 4 Portion of the experimental spectrum of *syn–anti*-CDIT (upper black trace) showcasing the resolution of the hyperfine structure. The simulation (lower purple trace) based on fitted rotational parameters reproduces the hyperfine splitting at a rotational temperature of 0.5 K.

 This journal is © the Owner Societies 2024

Published on 18 September 2024. Downloaded on 04.02.2026 19:17:07.

can be estimated from the relative intensities of their rotational transitions. According to the procedure described by Quesada-Moreno *et al.*,[34] a set of three or four rotational transitions of the two species with the same $J''_{K_a'' K_c''} \leftarrow J'_{K_a' K_c'}$ quantum numbers are selected, and their intensities are normalized by the square of the respective electric dipole moment. To get a reliable insight into the relative abundances, it is key that the selected transitions fall within a relatively narrow frequency range, *e.g.* up to 2 GHz. However, even though *syn–syn* and *syn–anti*-CDIT are conformers of the same compound, the experimentally determined A_0 rotational constants differ by an order of magnitude. In our rotational spectra there are no assigned transitions that fulfill these requirements and therefore this method would give an unreliable result.

An alternative procedure to estimate the relative abundances of the two species is to use the simulation function of PGOPHER.[26] The spectra of *syn–syn*- and *syn–anti*-CDIT were simulated simultaneously at a rotational temperature of 0.5 K, using the calculated $|\mu_b|$ dipole moment of 1.2 and 2.2 D, respectively. The rotational temperature of 0.5 K was selected as it can reproduce the experimental intensities of rotational transitions of each species individually. It should be noted that the rotational partition function of each molecule at the given temperature is by default taken into account when the intensities are simulated with PGOPHER. Finally, the simulated abundance of *syn–syn*-CDIT was set to 1 while the abundance of *syn–anti*-CDIT was adjusted until the relative intensities of the two simulations could reproduce those of the experimental spectrum. Following this procedure, it is estimated that *syn–syn*-CDIT is approximately 8 to 10 times more abundant than *syn–anti*-CDIT under the given experimental conditions.

The estimated 8 : 1 to 10 : 1 abundance ratio between *syn–syn*- and *syn–anti*-CDIT is consistent with the computed relative energies of the two at the B3LYP-D3(BJ)/aug-cc-pVTZ level. The two conformers are separated by an energetic barrier of 16 kJ mol^{-1} with the local *syn–anti* minimum lying 4.5 kJ mol^{-1} higher than the global *syn–syn*-CDIT minimum. The *anti–anti* conformation is not identified in the spectrum collected under our experimental conditions. Despite the fact that *anti–anti*-CDIT possesses the largest $|\mu_b|$ electric dipole moment out of the three conformers, this conformation is energetically disfavored by lying 14 kJ mol^{-1} above the global minimum. The relative populations of the three conformers of CDIT can be calculated according to their Boltzmann distributions at the temperature of the sample during the experiment (75 °C/348 K), prior to collisional cooling due to supersonic expansion, and by considering their computed energies, relative to the global minimum. Using the expression $N/N_0 = \exp\left(-\frac{\Delta E}{kT}\right)$, where N/N_0 is the abundance ratio of two conformations, ΔE is the computed relative energy, k is the Boltzmann constant, and T is the temperature of the sample, we calculate that 80% of CDIT is in the *syn–syn* conformer, while the *syn–anti* and *anti–anti* conformers take up approximately 17% and 3%, respectively. Considering the double degeneracy of the *syn–anti*-CDIT, the relative abundance ratio of the two lowest energy conformers are approximately 80 : 34. The calculated abundances are broadly consistent with the estimated abundances from the rotational spectrum.

Table 4 An overview of the (*syn*–)*syn* to (*syn*–)*anti* ratio of CDIT and other related compounds, determined through different methods, alongside computed energy barriers

Compound	(*syn*–)*syn* : (*syn*–)*anti* ratio	ΔE (kJ mol^{-1})	Barrier (kJ mol^{-1})	Method
$CO(N_3)_2$[a]	88 : 12 (∼7 : 1)	5–6.7	40.6	Matrix IR, GED
$CO(NCO)_2$[b]	66 : 34 (∼2 : 1)	3.8(8)	12.6	GED
CDIT $CO(NCS)_2$[c]	10 : 1	2.9–4.5	8–16	CP-FTMW
F(C═O)NCO[d]	77 : 23	2.1–5.0	—	GED
Cl(C═O)NCO[e]	25(8) : 75(8)	1.7–6.7	—	GED
Br(C═O)NCO[f]	Mainly *anti*	—	—	IR and Raman
Cl(C═O)NCS[g]	84(6) : 16(6)	1.3	5.9	GED
Cl(C═O)SCN[g]	Mainly *syn*	7.1	38.9	IR

[a] Ratio, computed energy difference, and barrier to interconversion between *syn–syn*- and *syn–anti*-$CO(N_3)_2$ from ref. 24. [b] Ratio between *syn–syn*- to *syn–anti*-$CO(NCO)_2$ and energy difference and barrier from ref. 23 and 40. [c] *syn–syn*- to *syn–anti*-$CO(NCS)_2$ ratio determined in this work, computed energy difference and barrier to interconversion from this work and ref. 41. [d] Ratio from ref. 31, 33, 36 and 42, and computed energy and barrier from ref. 33, 36 and 42. [e] From ref. 36 and 42. [f] From ref. 37 the ratio is not explicitly determined, however, the *anti*-conformer is favoured. Decreased electronegativity of the halogen atom [χ(F) > χ(Cl) > χ(Br)] favors the adoption of an *anti*-orientation of the –NCO group. [g] From ref. 39.

Previous studies have explored the conformational equilibrium of compounds structurally related to CDIT, both in the condensed and gas phase. A summary of their determined relative abundances as well as their barriers to interconversion are summarized in Table 4. Compounds with the general formula X(C═O)NCO (X = F, Cl, Br) consist of a central carbonyl group, which is substituted by a halogen atom and a pseudohalide group. In relation to CDIT, those can also exist as different rotational conformers: *syn* and *anti* (see Fig. 1). Both IR and Raman spectroscopy for fluoro,[31–33,35] chloro,[32,36] and bromocarbonyl[37] isocyanate show that their conformers are in an equilibrium state at room temperature. For X = F the *syn* conformer is with 75(12)%[33] preferred, according to gas phase electron diffraction (GED), while for X = Cl, and X = Br the *anti*-conformer is the dominant form. The *syn* to *anti* ratio for chlorocarbonyl isocyanate calculated from GED is 25(8) : 75(8).[36]

Fluoro- and chlorocarbonyl isothiocyanate (X(C═O)NCS (X = F, Cl))[38] as well as their isomers, fluoro- and chlorocarbonyl thiocyanate (X(C═O)SCN (X = F, Cl)),[39] also show an equilibrium state in the gas and liquid phase. In the solid state, solely the thermodynamically more stable *syn* conformers of F(C═O)NCS, F(C═O)SCN, Cl(C═O)SCN are present, as it was deduced from single-crystal XRD and solid-state Raman spectroscopy. The structure of Cl(C═O)NCS was determined by GED and the conformer *syn* to *anti* ratio is 84(6) : 16(6),[39] being the only determined ratio. As already discussed, CDIT and its related dipseudohalides, carbonyl diisocyanate ($CO(NCO)_2$) and carbonyl diazide ($CO(N_3)_2$), can in principle exist as three different conformers: *syn–syn*, *syn–anti*, and *anti–anti* (see Fig. 1).[22]

Published on 18 September 2024. Downloaded on 04.02.2026 19:17:07.

Both $CO(NCO)_2$ and $CO(N_3)_2$ show an equilibrium in the gas phase between their *syn–syn* and *syn–anti* conformers with a ratio of 62 : 38[40] and 88 : 12[24] (values estimated from IR spectroscopy), respectively. For carbonyl diisocyanate the ratio was refined from GED and is 66(3) : 34(3).[23] These values fit well with the computed energy difference of 4.3 kJ mol^{-1} and 6.9 kJ mol^{-1} (B3LYP/6-311+G(3d,f) level of theory) between the *syn–syn*- and *syn–anti*-conformers of $CO(NCO)_2$ and $CO(N_3)_2$, respectively.[23,24,40] For both compounds, the *anti–anti* conformer is not found spectroscopically, probably as it lies much higher in energy, as a result of steric repulsion between the pseudohalide groups both being *anti* oriented with respect to the carbonyl group. In the solid state, both crystallize with their thermodynamically stable rotamer, which is the *syn–syn* conformer.[23,24] Pfeiffer *et al.*[41] discussed a correlation between the *syn–syn* to *syn–anti* conformational ratio and the computed energy difference between conformers. The general trend suggests that a higher *syn–syn* to *syn–anti* ratio is consistent with a higher energy difference between the two conformers. From Table 4, we also observe that a higher ratio is associated with a lower energy barrier to interconversion, suggesting a lower conversion rate to *syn–anti*, and the findings for CDIT fit well with this observation.

Nuclear quadrupole coupling constants

The nuclear quadrupole coupling constants determined for *syn–syn*- and *syn–anti*-CDIT were diagonalized according to a common set of orthogonal *x*, *y*, *z* axes. These are positioned on each individual N nucleus, yielding the diagonalized χ_{xx}, χ_{yy}, and χ_{zz} constants summarized in Table 5. The diagonalization was performed with QDIAG,[43] and a visualization of the orientation of the axes is shown in Fig. S1 in the ESI.† The off-diagonal $|\chi_{ab}|$ constants were obtained through DFT calculations at the B3LYP-D3(BJ)/aug-cc-pVTZ level and given a 10% uncertainty. The same procedure was performed for other related compounds with a N nucleus within a –NCS group as well as for compounds with a $–NH_2$ group. The calculated values of $|\chi_{ab}|$ are given in the footnotes of Table 5.

From the values in Table 5, we observe that the local electronic environment of a N nucleus in a –NCS group displays significant differences to that of a $–NH_2$ group, *e.g.*, in phenyl isothiocyanate (Ph-NCS)[44] and urea.[45] These differences can be partially rationalized by looking at the chemical environment around each N nucleus. In the case of the molecules with one or more –NCS groups, the N atom exhibits sp hybridization in a linear arrangement with the neighboring atoms, while the N atom in $–NH_2$ is sp^3 hybridized in a slightly pyramidal configuration. Comparing *syn–syn*- and *syn–anti*-CDIT to the structurally related urea, the magnitude of $|\chi_{zz}|$, which in a planar or almost planar molecule is approximately equal to $|\chi_{cc}|$, provides an indication of the degree of delocalization of the electron pair on the N nucleus. The –NCS group can contribute to resonance forms and, in combination with the electron withdrawing character of the group and the higher electronegativity of the S atom, the lone pair of N exhibits a higher degree of delocalization. The more localized electron pair in $–NH_2$ is reflected by the significantly larger magnitude of $|\chi_{zz}|$. The closely related molecules to CDIT, ethoxycarbonyl isothiocyanate[46] and Ph–NCS,[44] display a similar electronic environment around the N nucleus suggesting that the component attached to the –NCS group has little effect on the local electronic environment of the N nucleus. *Syn–syn* and *syn–anti*-CDIT exhibit similar electronic environments around the N nuclei, suggesting that the reactivity of the molecule is not exclusively associated with a certain conformer. However, following the earlier arguments around the relative abundances, the *syn–syn* form is expected to partake in most reactions.

Structural analysis

Experimental determination of the rotational constants of the parent *syn–syn*-CDIT (Table 2) and its singly substituted ^{34}S, ^{13}C, and ^{15}N isotopologues (Table 3) allows for Kraitchman[48,49] analysis to be performed to obtain the substitution (r_s) coordinates of the atoms in the –NCS groups. The analysis was performed with the program KRA from the PROSPE website.[43] The resulting r_s coordinates, alongside their fractional uncertainties[50] to partially account for rotation–vibration effects, are shown in Table 6. The r_s method can only provide the magnitude of each coordinate, so the signs were inferred from the calculated DFT geometry. The $|c|$ coordinates were calculated as zero, consistent with planarity of the molecule, which is also supported by the value of the inertia defect[51] $\Delta_0 = I_c - I_a - I_b$ = –0.182 u $Å^2$, where I_x corresponds to the respective moment of inertia for each axis. The magnitude and the sign of Δ_0 is consistent with low-lying out-of-plane motions of the –NCS

Table 5 Diagonalized nuclear quadrupole coupling constants χ_{xx}, χ_{yy}, and χ_{zz} for CDIT and other related compounds

		χ_{xx} (MHz)	χ_{yy} (MHz)	χ_{zz} (MHz)
syn–syn-CDIT[a]	N_3/N_6	−1.790(81)	2.382(81)	−0.5924(60)
syn–anti-CDIT[a]	N_3	−2.24(16)	2.79(16)	−0.554(12)
	N_6	−1.87(21)	2.31(21)	−0.441(13)
Ethoxycarbonyl isothiocyanate[b]	N	−1.685(86)	2.338(86)	−0.6532(25)
Ph–NCS[c]	N	−1.4635	1.94656	−0.483069
Aniline[d]	N	4.20(13)	0	−4.20(6)
Urea[e]	N	2.311(18)	1.778(18)	−4.0889(26)

[a] This work. Calculated off-diagonal components for *syn–syn*-CDIT $|\chi_{ab}(N_3/N_6)|$ = 1.30(13) MHz and for *syn–anti*-CDIT $|\chi_{ab}(N_3)|$ = 2.04(20) MHz and $|\chi_{ab}(N_6)|$ = 2.08(21) MHz at the B3LYP-D3(BJ)/aug-cc-pVTZ level. [b] Calculated off-diagonal component $|\chi_{ab}|$ = 1.33(13) MHz at the B3LYP-D3(BJ)/aug-cc-pVTZ level and from ref. 46. [c] From ref. 44. [d] Calculated off-diagonal component $|\chi_{ab}|$ = 2.09(12) MHz at the B3LYP-D3(BJ)/aug-cc-pVTZ level and from ref. 47. [e] Calculated off-diagonal component $|\chi_{ab}|$ = 0.215(22) MHz at the B3LYP-D3(BJ)/aug-cc-pVTZ level and from ref. 45.

 This journal is © the Owner Societies 2024

Published on 18 September 2024. Downloaded on 04.02.2026 19:17:07.

Table 6 Atomic substitution (r_s) coordinates of *syn–syn*-CDIT determined experimentally alongside the calculated (r_e) coordinates, and structural parameters determined with XRD and CP-FTMW spectroscopy

syn–syn-CDIT		$\lvert a\rvert$[a] (Å)	b (Å)
N	r_e	1.1426	−0.4410
	r_s	1.087(12)	−0.4273(35)
C	r_e	2.3366	−0.2639
	r_s	2.3302(12)	−0.2690(56)
S	r_e	3.8920	−0.1624
	r_s	3.8687(13)	−0.086(17)

	XRD	r_s
C═O (Å)	1.181(16)	—
$C_{carbonyl}$–N (Å)	1.381(5)	—
N═C (Å)	1.207(4)	1.253(12)
C═S (Å)	1.526(4)	1.5497(28)
∠(SCN) (°)	173.7(4)–175.7(4)	179.5(8)

[a] Only the magnitude of the *a*-coordinates is provided here. Due to the C_{2v} symmetry, to describe the positions of the atoms in either one of the –NCS groups, the *a*-coordinates need to all carry a positive or negative sign, respectively.

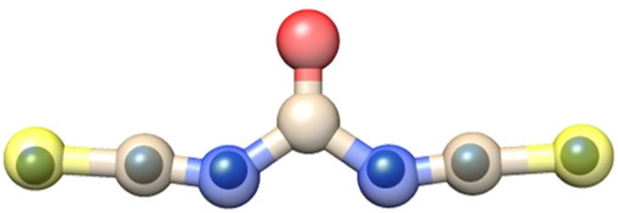

Fig. 5 The experimental r_s coordinates (solid spheres) of *syn–syn*-CDIT compared to the calculated B3LYP-D3(BJ)/aug-cc-pVTZ r_e coordinates (translucent underlying structure).

groups at the zero point. The r_s coordinates were evaluated with EVAL[43] to yield bond lengths and angles relevant to the –NCS groups and are summarized in Table 6.

The experimentally determined r_s coordinates are shown alongside the r_e calculated coordinates in Table 6 and Fig. 5. The high level of agreement between the two provides strong evidence in support of the geometry for *syn–syn*-CDIT. The values of the r_s bond lengths r(C═S) and r(N═C), and the angle ∠(SCN) are compared to those determined by single-crystal X-ray diffraction (XRD).[21] A slight elongation of all determined bond lengths is observed for the gas phase structure while the ∠(SCN) angle shows an essentially linear arrangement in the atoms of the –NCS groups. The more compact structure as well as the slight distortion from linearity in the ∠(SCN) angle that is observed with XRD is likely due to packing effects in the crystal. It is worth noting that only the *syn–syn* conformer crystallizes and therefore there is no structural information for the *syn–anti* conformer.[21]

Conclusions

The rotational spectra of two conformers of the reactive compound carbonyl diisothiocyanate, *syn–syn* and *syn–anti*, were recorded with chirped pulse Fourier transform microwave spectroscopy in the 2–12 GHz frequency region. We estimate that the *syn–syn* form is approximately eight to ten times more abundant than the *syn–anti* form, which fits well with the observed relative abundances of conformers of other related compounds. The spectrum of *syn–syn*-carbonyl diisothiocyanate was manifested as two distinct nuclear spin isomers, *ortho* and *para*, that exhibit characteristics of nuclear spin statistics for bosons, and were identified by the varying hyperfine structure of their rotational transitions. Observation of singly substituted isotopologues allowed for partial structure determination of *syn–syn*-carbonyl diisothiocyanate and determination of the atomic coordinates of the atoms in the –NCS groups. The gas-phase structure of isolated *syn–syn*-carbonyl diisothiocyanate shows a slight elongation of the bond lengths between the atoms of the –NCS groups when compared to the structure determined with XRD using crystals.

Carbonyl diisothiocyanate is a unique example of a molecule composed exclusively of eight bosons (I = 0 and 1), six of which, in the *syn–syn* and *anti–anti* forms, appear as three equivalent pairs (–NCS groups). *Syn–syn*-carbonyl diisothiocyanate is present as two nuclear spin isomers, *ortho* and *para*, which are distinguished by their nuclear quadrupole coupling signatures, as an outcome of differing symmetries in their nuclear states while their nuclear quadrupole coupling constants χ_{aa} and χ_{bb}–χ_{cc} are the same for the two nuclear spin isomers, as seen in Table 3. Observation of *ortho* and *para* nuclear spin isomers in molecules that exhibit nuclear spin statistics for bosons have previously been reported for several systems, however, these mainly include small linear molecules[52,53] (*e.g.*, D_2, N_2) and asymmetric tops such as non-covalently bound complexes[54–56] (*e.g.*, CO···N_2, N_2···HCl, N_2···OCS) where the C_2 axis coincides with the *a*-axis of inertia. In terms of nuclear spin statistics, these complexes were shown to exhibit characteristics of their respective boson counterparts that exchange upon a C_2 rotation about the symmetry axis, and the linkage between their nuclear spin isomers lies within the J and K_a quantum numbers. In the case of *syn–syn*-carbonyl diisothiocyanate, the C_2 axis is aligned with the *b*-axis of inertia, meaning that inclusion of the K_c quantum number is necessary to link the two isomers. Considering the lack of examples of complex molecules in the literature with nuclear spin isomers where the J, K_a, and K_c quantum numbers are required to properly describe them, *syn–syn*-carbonyl diisothiocyanate makes for a noteworthy case.

Data availability

The data supporting this article have been included as part of the ESI.† Lists of fitted transition frequencies as well as detailed operator codes used in the fits are summarized in the ESI.†

Conflicts of interest

There are no conflicts to declare.

Published on 18 September 2024. Downloaded on 04.02.2026 19:17:07.

Acknowledgements

J. P. acknowledges *Fonds der chemischen Industrie* for a PhD scholarship. F. T. acknowledges funding through the *German Research Council (DFG) TA 1357/5-1*. The authors would like to thank Prof. Dr Daniel Obenchain for his help in constructing the input files for SPFIT/SPCAT. The authors would also like to thank Dr Denis Tikhonov for useful discussions around the NEB calculations.

References

1 L. D. Landau and E. M. Lifshitz, *Quantum mechanics: non-relativistic theory*, Elsevier, 2013, vol. 3.
2 E. Moreno-Pineda, M. Damjanović, O. Fuhr, W. Wernsdorfer and M. Ruben, Nuclear Spin Isomers: Engineering a $Et_4N[DyPc_2]$ Spin Qudit, *Angew. Chem., Int. Ed.*, 2017, **56**, 9915–9919.
3 A. Gaita-Ariño, F. Luis, S. Hill and E. Coronado, Molecular spins for quantum computation, *Nat. Chem.*, 2019, **11**, 301–309.
4 S. S. Kaushik, Z. I. Cleveland, G. P. Cofer, G. Metz, D. Beaver, J. Nouls, M. Kraft, W. Auffermann, J. Wolber, H. P. McAdams and B. Driehuys, Diffusion-weighted hyperpolarized ^{129}Xe MRI in healthy volunteers and subjects with chronic obstructive pulmonary disease, *Magn. Reson. Med.*, 2011, **65**, 1154–1165.
5 J. R. Birchall, M. R. H. Chowdhury, P. Nikolaou, Y. A. Chekmenev, A. Shcherbakov, M. J. Barlow, B. M. Goodson and E. Y. Chekmenev, Pilot Quality-Assurance Study of a Third-Generation Batch-Mode Clinical-Scale Automated Xenon-129 Hyperpolarizer, *Molecules*, 2022, **27**, 1327.
6 T. Hama, A. Kouchi and N. Watanabe, Statistical *ortho*-to-*para* ratio of water desorbed from ice at 10 kelvin, *Science*, 2016, **351**, 65–67.
7 H. Kawakita, J. Watanabe, H. Ando, W. Aoki, T. Fuse, S. Honda, H. Izumiura, T. Kajino, E. Kambe, S. Kawanomoto, K. Noguchi, K. Okita, K. Sadakane, B. Sato, M. Takada-Hidai, Y. Takeda, T. Usuda, E. Watanabe and M. Yoshida, The Spin Temperature of NH_3 in Comet C/1999S4 (LINEAR), *Science*, 2001, **294**, 1089–1091.
8 J. E. Dickens and W. M. Irvine, The Formaldehyde *Ortho*/*Para* Ratio as a Probe of Dark Cloud Chemistry and Evolution, *Astrophys. J.*, 1999, **518**, 733–739.
9 K. F. Bonhoeffer and P. Harteck, Experimente über *Para*- und *Ortho*wasserstoff, *Naturwissenschaften*, 1929, **17**, 182.
10 D. A. Horke, Y.-P. Chang, K. Długołęcki and J. Küpper, Separating *Para* and *Ortho* Water, *Angew. Chem., Int. Ed.*, 2014, **53**, 11965–11968.
11 P. Cacciani, J. Cosléou and M. Khelkhal, Nuclear spin conversion in H_2O, *Phys. Rev. A: At., Mol., Opt. Phys.*, 2012, **85**, 12521.
12 Z.-D. Sun, M. Ge and Y. Zheng, Separation and conversion dynamics of nuclear-spin isomers of gaseous methanol, *Nat. Commun.*, 2015, **6**, 6877.
13 P. L. Chapovsky, J. Cosléou, F. Herlemont, M. Khelkhal and J. Legrand, Separation and conversion of nuclear spin isomers of ethylene, *Chem. Phys. Lett.*, 2000, **322**, 424–428.
14 Z.-D. Sun, K. Takagi and F. Matsushima, Separation and Conversion Dynamics of Four Nuclear Spin Isomers of Ethylene, *Science*, 2005, **310**, 1938–1941.
15 P. L. Chapovsky, V. V. Zhivonitko and I. V. Koptyug, Conversion of Nuclear Spin Isomers of Ethylene, *J. Phys. Chem. A*, 2013, **117**, 9673–9683.
16 B. Nagels, M. Schuurman, P. L. Chapovsky and L. J. F. Hermans, Nuclear spin conversion in molecules: experiments on $^{13}CH_3F$ support a mixing-of-states model, *Phys. Rev. A: At., Mol., Opt. Phys.*, 1996, **54**, 2050.
17 P. L. Chapovskii, Conversion of nuclear spin modifications of CH_3F molecules in the gaseous phase, *Sov. J. Exp. Theor. Phys.*, 1990, **70**, 895.
18 A. E. Dixon, The action of metallic thiocyanates upon carbonyl chloride, *Proc. R. Soc. London*, 1902, **18**, 235.
19 R. Bunnenberg and J. C. Jochims, Carbonyldiisothiocyanat, *Chem. Ber.*, 1981, **114**, 2075–2086.
20 R. Bunnenberg, J. C. Jochims and H. Härle, Zur Darstellung und Chlorierung von Carbonyl-diisothiocyanat, *Chem. Ber.*, 1982, **115**, 3587–3596.
21 J. Pfeiffer, C. Trost, A. Pachkovska and F. Tambornino, A Crystallographic, Spectroscopic, and Computational Investigation of Carbonyl and Oxalyl Diisothiocyanate, *Inorg. Chem.*, 2021, **60**, 10722–10728.
22 W. J. Balfour, S. G. Fougere, D. Klapstein and W. M. Nau, The infrared and Raman spectra of carbonyl diisocyanate, *Spectrochim. Acta, Part A*, 1994, **50**, 1039–1046.
23 T. M. Klapötke, B. Krumm, S. Rest, R. Scharf, J. Schwabedissen, H.-G. Stammler and N. W. Mitzel, Carbonyl Diisocyanate $CO(NCO)_2$: Synthesis and Structures in Solid State and Gas Phase, *J. Phys. Chem. A*, 2016, **120**, 4534–4541.
24 X. Zeng, M. Gerken, H. Beckers and H. Willner, Synthesis and Characterization of Carbonyl Diazide, $OC(N_3)_2$, *Inorg. Chem.*, 2010, **49**, 9694–9699.
25 J. K. G. Watson, Determination of Centrifugal Distortion Coefficients of Asymmetric-Top Molecules. III. Sextic Coefficients, *J. Chem. Phys.*, 2003, **48**, 4517–4524.
26 C. M. Western, PGOPHER: a program for simulating rotational, vibrational and electronic spectra, *J. Quant. Spectrosc. Radiat. Transfer*, 2017, **186**, 221–242.
27 G. S. Grubbs II, D. A. Obenchain, H. M. Pickett and S. E. Novick, H_2-AgCl: a spectroscopic study of a dihydrogen complex, *J. Chem. Phys.*, 2014, **141**, 114306.
28 H. M. Pickett, The fitting and prediction of vibration-rotation spectra with spin interactions, *J. Mol. Spectrosc.*, 1991, **148**, 371–377.
29 R. F. Code and N. F. Ramsey, Molecular-Beam Magnetic Resonance Studies of HD and D_2, *Phys. Rev. A: At., Mol., Opt. Phys.*, 1971, **4**, 1945–1959.
30 D. W. Ball, Carbonyl diazide, $OC(N_3)_2$: calculated thermodynamic properties, *Comput. Theor. Chem.*, 2011, **965**, 176–179.
31 D. Klapstein and W. M. Nau, Conformational properties of carbonyl isocyanates—stereoelectronic effects favouring the cisoid conformation, *J. Mol. Struct.*, 1993, **299**, 29–41.

 This journal is © the Owner Societies 2024

Published on 18 September 2024. Downloaded on 04.02.2026 19:17:07.

32 D. Klapstein and W. M. Nau, Spectroscopy of acyl and carbonyl isocyanates, *Spectrochim. Acta, Part A*, 1994, **50**, 307–316.
33 H.-G. Mack, C. O. Della Védova and H. Willner, Structures and conformations of carbonyl isocyanates and carbonyl azides. An experimental and theoretical investigation, *J. Mol. Struct.*, 1993, **291**, 197–209.
34 M. M. Quesada-Moreno, A. Krin and M. Schnell, Analysis of thyme essential oils using gas-phase broadband rotational spectroscopy, *Phys. Chem. Chem. Phys.*, 2019, **21**, 26569–26579.
35 J. R. Durig, G. A. Guirgis, K. A. Krutules, H. Phan and H. D. Stidham, Raman and infrared spectra, conformational stability, barriers to internal rotation and ab initio calculations of fluorocarbonyl isocyanate, *J. Raman Spectrosc.*, 1994, **25**, 221–232.
36 H.-G. Mack, H. Oberhammer and C. O. Della Védova, How reliable are *ab initio* calculations? Experimental and theoretical investigation of the structure and conformation of chlorocarbonyl isocyanate, ClC(O)NCO, *J. Mol. Struct.: THEOCHEM*, 1989, **200**, 277–288.
37 C. O. D. Védova, Preparation and properties of bromocarbonyl isocyanate, BrC(O)NCO, *Spectrochim. Acta, Part A*, 1992, **48**, 1179–1185.
38 L. A. Ramos, S. E. Ulic, R. M. Romano, M. F. Erben, C. W. Lehmann, E. Bernhardt, H. Beckers, H. Willner and C. O. Della Védova, Vibrational Spectra, Crystal Structures, Constitutional and Rotational Isomerism of FC(O)SCN and FC(O)NCS, *Inorg. Chem.*, 2010, **49**, 11142–11157.
39 L. A. Ramos, S. E. Ulic, R. M. Romano, M. F. Erben, Y. V. Vishnevskiy, C. G. Reuter, N. W. Mitzel, H. Beckers, H. Willner, X. Zeng, E. Bernhardt, M. Ge, S. Tong and C. O. Della Védova, Spectroscopic Characterization and Constitutional and Rotational Isomerism of ClC(O)SCN and ClC(O)NCS, *J. Phys. Chem. A*, 2013, **117**, 2383–2399.
40 Q. Liu, H. Li, Z. Wu, D. Li, H. Beckers, G. Rauhut and X. Zeng, Photolysis of Carbonyl Diisocyanate: Generation of Isocyanatocarbonyl Nitrene and Diazomethanone, *Chem. – Asian J.*, 2016, **11**, 2953–2959.
41 J. Pfeiffer, J. P. Wagner and F. Tambornino, Photolytic Decarbonylation of Oxalyl Diisothiocyanate in Solid Argon Matrices to *syn–anti* Carbonyl Diisothiocyanate and its Isomerization, *Eur. J. Inorg. Chem.*, 2023, e202300290.
42 M. Tho Nguyen, M. R. Hajnal and L. G. Vanquickenborne, How reliable are *ab initio* calculations?, *J. Mol. Struct.: THEOCHEM*, 1991, **231**, 185–193.
43 Z. Kisiel, PROSPE – Programs for ROtational SPEctroscopy, 2024, **https://info.ifpan.edu.pl/~kisiel/prospe.htm**.
44 W. Sun, W. G. D. P. Silva and J. van Wijngaarden, Rotational Spectra and Structures of Phenyl Isocyanate and Phenyl Isothiocyanate, *J. Phys. Chem. A*, 2019, **123**, 2351–2360.
45 U. Kretschmer, D. Consalvo, A. Knaack, W. Schade, W. Stahl and H. Dreizler, The ^{14}N quadrupole hyperfine structure in the rotational spectrum of laser vaporized urea observed by molecular beam Fourier transform microwave spectroscopy, *Mol. Phys.*, 1996, **87**, 1159–1168.
46 Y. Xu, W. Li, J. Zhang and G. Feng, Conformations and structures of ethoxycarbonyl isothiocyanate revealed by rotational spectroscopy, *Chin. J. Chem. Phys.*, 2022, **35**, 875–882.
47 A. Hatta, M. Suzuki and K. Kozima, Nuclear Quadrupole Effects in the Microwave Spectrum and Dipole Moment of Aniline, *Bull. Chem. Soc. Jpn.*, 1973, **46**, 2321–2323.
48 J. Kraitchman, Determination of Molecular Structure from Microwave Spectroscopic Data, *Am. J. Phys.*, 1953, **21**, 17–24.
49 H. D. Rudolph, Extending Kraitchman's equations, *J. Mol. Spectrosc.*, 1981, **89**, 430–439.
50 C. Costain, Further comments on the accuracy of rs substitution structures, *Trans. Am. Crystallogr. Assoc.*, 1966, **2**, 157–164.
51 R. K. Bohn, J. A. Montgomery, H. H. Michels and J. A. Fournier, Second moments and rotational spectroscopy, *J. Mol. Spectrosc.*, 2016, **325**, 42–49.
52 F. G. Brickwedde, R. B. Scott and H. S. Taylor, The Difference in Vapor Pressures of *Ortho* and *Para* Deuterium, *J. Chem. Phys.*, 1935, **3**, 653–660.
53 S. Fleischer, I. S. Averbukh and Y. Prior, Selective Alignment of Molecular Spin Isomers, *Phys. Rev. Lett.*, 2007, **99**, 93002.
54 C. Xia, A. R. W. McKellar and Y. Xu, Infrared spectrum of the CO–N_2 van der Waals complex: assignments for CO-*para*N_2 and observation of a bending state for CO-*ortho*N_2, *J. Chem. Phys.*, 2000, **113**, 525–533.
55 R. S. Altman, M. D. Marshall and W. Klemperer, The microwave spectrum and molecular structure of N_2–HCl, *J. Chem. Phys.*, 1983, **79**, 57–64.
56 J. P. Connelly, S. P. Duxon, S. K. Kennedy, B. J. Howard and J. S. Muenter, Hyperfine and Tunneling Effects in the Microwave Spectrum of N_2–OCS, *J. Mol. Spectrosc.*, 1996, **175**, 85–98.